Optimal periodic orbits of continuous time chaotic systems

Tsung-Hsun Yang*
Department of Physics, National Cheng Kung University, Tainan 70101, Taiwan

Brian R. Hunt
Department of Mathematics and Institute for Physical Science and Technology, University of Maryland, College Park, Maryland 20742

Edward Ott
Department of Electrical Engineering and Department of Physics, Institute for Plasma Research, University of Maryland, College Park, Maryland 20742

(Received 17 June 1999; revised manuscript received 17 February 2000)

In previous work [B. R. Hunt and E. Ott, Phys. Rev. Lett. **76**, 2254 (1996); Phys. Rev. E **54**, 328, (1996)], based on numerical experiments and analysis, it was conjectured that the *optimal orbit* selected from all possible orbits on a chaotic attractor is ''typically'' a periodic orbit of low period. By an optimal orbit we mean the orbit that yields the largest value of a time average of a given smooth ''performance'' function of the system state. Thus optimality is defined with respect to the given performance function. (The study of optimal orbits is of interest in at least three contexts: controlling chaos, embedding of low-dimensional attractors of high-dimensional dynamical systems in low-dimensional measurement spaces, and bubbling bifurcations of synchronized chaotic systems.) Here we extend this previous work. In particular, the previous work was for discrete time dynamical systems, and here we shall consider continuous time systems (flows). An essential difference for flows is that chaotic attractors can have embedded within them, not only unstable periodic orbits, but also unstable steady states, and we find that optimality can often occur on steady states. We also shed further light on the sense in which optimality is ''typically'' achieved at low period. In particular, we find that, as a system parameter is tuned to be closer to a crisis of the chaotic attractor, optimality may occur at higher period.

PACS number(s): 05.45.−a

I. INTRODUCTION

One strategy [1–6] for controlling chaotic systems by means of small controls is the following: first, determine unstable periodic orbits (UPOs) embedded in the chaotic attractor; then, examine the UPOs to determine which one gives the best system performance; and finally control the system to follow that orbit. In general the system performance averaged over time can be expressed as the time average of some function $F(x)$ of the system state x. We call F the performance function and denote its time average by $\langle F\rangle$,

$$\langle F\rangle = \lim_{T\to\infty}\frac{1}{T}\int_0^T F(x(t))dt, \tag{1a}$$

$$\langle F\rangle = \lim_{t\to\infty}\frac{1}{T}\sum_{t=1}^{T} F(x_t), \tag{1b}$$

where t denotes time and is either continuous [Eq. (1a)] or discrete [Eq. (1b)]. Thus the best, or optimal, orbit is the one yielding the largest value of $\langle F\rangle$ [7].

In this paper we shall be interested in the ''typical'' properties of optimal orbits. In previous work [8,9] this question was examined for the case of discrete time systems (maps), using a one-parameter family of performance functions, and considering typicality with respect to this parameter. Here we extend these considerations to continuous time systems (flows). In the previous work, numerical evidence for the following conjectures was presented using numerical experiments on one- and two-dimensional maps.

(i) The set of parameter values for which the optimal orbit is not periodic has Lebesgue measure zero; that is, the optimal orbit is periodic for almost every set of parameter values.

(ii) The Lebesgue measure of the set of parameter values for which the optimal orbit is periodic with a period equal to or larger than some value p decreases exponentially as $p\to\infty$. In this sense it was stated that optimality typically occurs at low period. (In the rest of the paper, whenever we refer to *low period* as being *typical*, it will be in this sense.)

(iii) Even when optimality occurs at very high period, there are usually fairly low-period orbits whose performance is only slightly less than that achieved by the optimal high-period orbit.

In the past, experimentalists working on controlling chaos have often experimentally determined only low-period unstable periodic orbits contained in the chaotic attractor. This is partly because the determination of many high-period unstable periodic orbits can be very demanding and in many cases is not feasible. The work of Refs. [8,9] indicates that there will usually be little gain, and often none, by going to the considerable effort of determining many more unstable periodic orbits.

Another possible motivation for consideration of optimal periodic orbits comes from the theory of embedding. Embed-

*Email address: thyang@mail.phys.ncku.edu.tw

ding is of particular interest for the analysis of experimental data from high- (including infinite-) dimensional dynamical systems. In particular, it has been shown [10,11] that, if D_L denotes the largest Lyapunov dimension of any orbit contained within an attractor and n is an integer greater than $2D_L$, then a generic embedding into an n-dimensional Euclidean space gives a one-to-one representation of the attractor. The Lyapunov dimension of an orbit is a function of its Lyapunov exponents, which are time averages in a more generalized sense than we consider in this paper. Thus the results described above *suggest* that the largest (optimal) Lyapunov dimension is typically attained on a periodic orbit with low period. Still another motivation for consideration of optimal periodic orbits is that they play a crucial role in the stability of synchronization of chaotic systems. In particular, they determine the onset of the ''bubbling transition'' (see Refs. [12]).

Is there any change in the results of the previous work on optimal periodic orbits if we consider a continuous time system? Although the trajectories of continuous systems can be reduced to discrete mappings by a Poincaré surface of section, the interval of continuous time between successive encounters with the surface of section varies with the starting point x on the surface of section. For such x, let $T(x)$ denote the time for the orbit from x to next intersect the surface of section; we call $T(x)$ the *return time* of x. Let $\tilde{F}(x)$ denote the time average of the performance function F over this time interval,

$$\tilde{F}(x)=\frac{1}{T(x)}\int_0^{T(x)} F(\tilde{x}(t))dt, \tag{2}$$

where $\tilde{x}(0)=x$. We can then express Eq. (1a) as

$$\langle F\rangle=\lim_{n\to\infty}\frac{\sum_{m=1}^{n} T(x_m)\tilde{F}(x_m)}{\sum_{m=1}^{n} T(x_m)}, \tag{3}$$

where the integer index m enumerates the surface of section piercings.

These considerations are complete as long as there are no steady states embedded in the attractor. If there are steady states, then it is possible to have initial conditions on the surface of section that generate orbits that go to the steady state (assumed to lie off the surface of section) without ever returning to the surface of section. In this case, $T(x)$ tends to infinity as x approaches an initial condition going to a steady state.

When steady states are present, we find that conjectures (i)–(iii), stated above for the case of maps, need to be modified. In particular, we conjecture that for continuous time systems, optimality typically occurs either on an unstable periodic orbit with low period or on an unstable steady state (if one exists in the chaotic attractor under consideration).

In Sec. II, we use map models to consider the case where $T(x)$ is finite for all x. This corresponds to the case where the attractor of the continuous time system has no embedded steady states. In Sec. III, we use the same maps but allow $T(x)\to\infty$ as x approaches some $\bar{x}$ to model the presence of a steady state in the flow.

In Sec. IV, we consider the Lorenz equations [13,14] as an example of a continuous time system with an embedded steady state. In this context, an interesting fact was recently pointed out by Zoldi and Greenside [15]: if one uses the parameters originally investigated by Lorenz, then, for the performance function Zoldi and Greenside studied, optimality occurs at a rather large period. This motivates us to examine the sense of the word ''typically'' in the statement that optimal orbits typically occur at low period. We find that, by enlarging the meaning of typicality to be with respect to both variation of system parameters and performance function parameters, it is still the case that optimality typically occurs at low period (or on a steady state).

II. DISCRETE MAPS WITH BOUNDED RETURN TIME

In [8,9] the discrete time average (1b) was considered for two one-dimensional maps, the doubling transformation and the tent map, using the one-parameter family of performance functions,

$$F_\gamma(x)=\cos[2\pi(x-\gamma)], \tag{4}$$

where $0\leqslant\gamma\leqslant 1$. The average thus considered is equivalent to the average (3) with $\tilde{F}$ replaced by F_γ and $T(x)\equiv 1$. In this section we will explore the effect of a nonconstant return time $T(x)$ on the average (3) using the smoothly varying function,

$$T_\varepsilon(x)=1+\varepsilon\sin 2\pi x, \tag{5}$$

for various ε between 0 and 1. As described in the Introduction, this type of return time function mimics the case of a Poincaré section of a continuous time attractor with no embedded steady states.

The average we consider in this section is thus

$$\langle F_\gamma\rangle_\varepsilon=\lim_{n\to\infty}\frac{\sum_{m=1}^{n} T_\varepsilon(x_m)F_\gamma(x_m)}{\sum_{m=1}^{n} T_\varepsilon(x_m)}, \tag{6}$$

with F_γ and T_ε defined above.

A. Doubling transformation

The first map we consider is the doubling transformation,

$$x_{n+1}=2x_n(\mathrm{mod}\ 1). \tag{7}$$

For each of the values $\varepsilon=0,0.1,0.2,\ldots,1.0$ we performed the following numerical experiment. For each of 10^5 evenly spaced values of γ between 0 and 1, we calculated the maximum value of $\langle F_\gamma\rangle_\varepsilon$ among all the periodic orbits of Eq. (7) with periods 1 to 24. Figure 1 shows the period of the optimal orbit as a function of the parameter γ for $\varepsilon=0.1$ and 0.5. The results are very similar to those in [8,9], which correspond to $\varepsilon=0$. As ε increases, the figure becomes less symmetric, but there is little qualitative change.

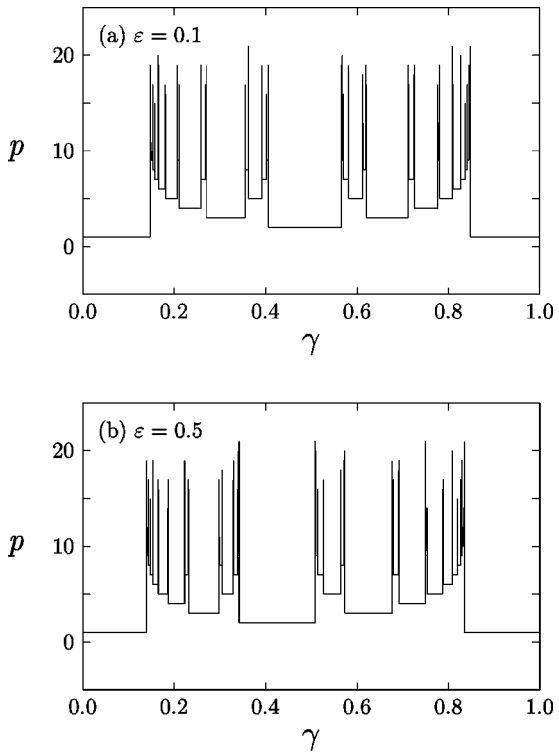

FIG. 1. Periods that optimize $\langle F_\gamma \rangle_\varepsilon$ for the doubling transformation with bounded return time $T(x_n) = 1 + \varepsilon \sin 2\pi x_n$, for (a) $\varepsilon = 0.1$ and (b) $\varepsilon = 0.5$.

To be more precise, let $r(p)$ be the fraction of γ values for which period p or larger is optimal. Figure 2 shows, for various ε, a test of the asymptotic prediction [8,9]

$$r(p) \leqslant K p^2 2^{-p},$$

where K is a fitting constant. Specifically, Fig. 2 shows plots of $\log_{10}[r(p)/p^2]$ versus p, which are to be compared to the dotted plot of $\log_{10}(2^{-p})$ versus p. The two agree well. We conclude that the conjecture that $r(p)$ decays exponentially as p increases is demonstrated by our results for all values of ε between 0 and 1.

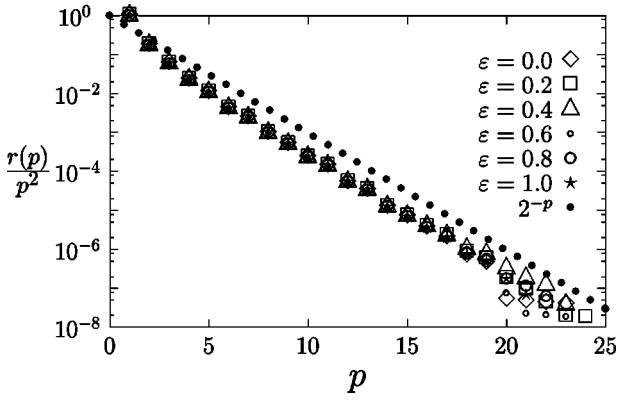

FIG. 2. Comparison of $r(p)/p^2$ with 2^{-p}, where $r(p)$ is the fraction of γ values for which period p or larger optimizes $\langle F_\gamma \rangle_\varepsilon$ for the doubling transformation with bounded return time $T(x_n) = 1 + \varepsilon \sin 2\pi x_n$.

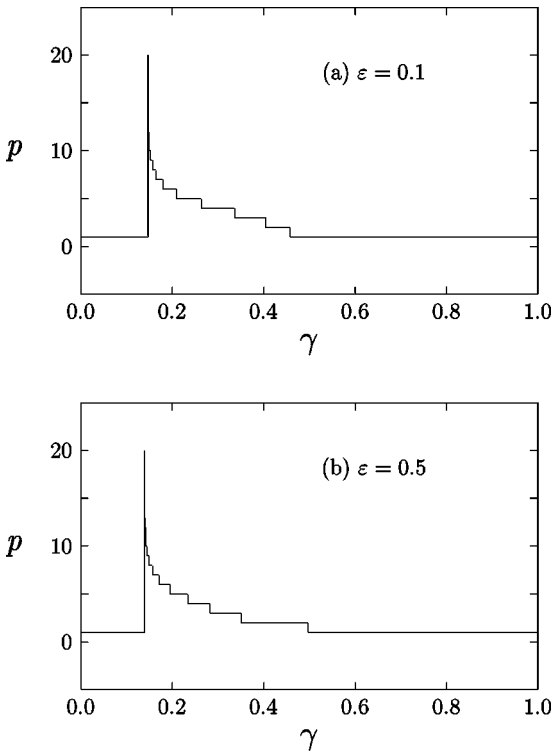

FIG. 3. Periods that optimize $\langle F_\gamma \rangle_\varepsilon$ for the tent map with bounded return time $T(x_n) = 1 + \varepsilon \sin 2\pi x_n$, for (a) $\varepsilon = 0.1$ and (b) $\varepsilon = 0.5$.

B. Tent map

Next, we consider the tent map on $[0,1]$,

$$x_{n+1} = \begin{cases} 2x_n, & x_n \leqslant \frac{1}{2} \\ 2(1-x_n), & x_n > \frac{1}{2}, \end{cases} \tag{8}$$

with the same time function (5) and performance function (4). We performed the same numerical experiment for various values of ε: for each of 10^5 evenly spaced values of γ between 0 and 1, we maximized the average (6) over all periodic orbits of Eq. (8) with period at most 24. For $\varepsilon = 0.1$ and $\varepsilon = 0.5$, the optimal period as a function of γ is shown in Fig. 3. Again, the results differ very little from those in [8,9] ($\varepsilon = 0$). The precise values of γ for which a given period is optimal shift slightly as ε increases, but the proportion $f(p)$ of γ values for which period p is optimal changes little except for the smallest values of p. Figure 4 shows the dependence of $r(p)$ on p for $\varepsilon = 0, 0.2, \ldots, 1.0$. Again, the values and the exponential decay of $r(p)$ across the intermediate values of p are consistent as ε changes.

III. DISCRETE MAPS WITH UNBOUNDED RETURN TIME

In this section, we explore the effect of unbounded return time on the problem of optimizing the average (6), using the maps (7) and (8) and performance function (4) from Sec. II together with a new family of return time functions $T_\varepsilon(x)$ that have a singularity $T_\varepsilon(x) \to \infty$ as x approaches a point $\overline{x}$.

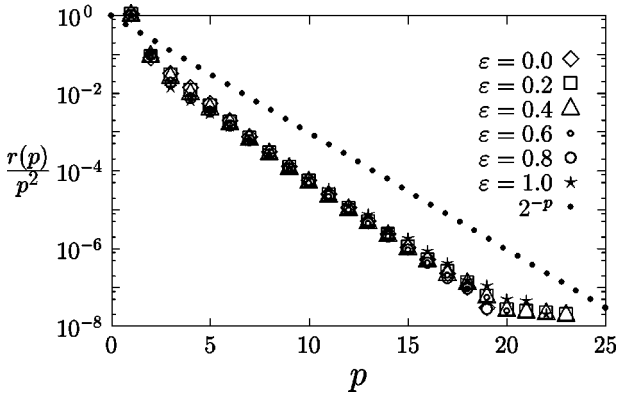

FIG. 4. Comparison of $r(p)/p^2$ with 2^{-p}, where $r(p)$ is the fraction of γ values for which period p or larger optimizes $\langle F_\gamma \rangle_\varepsilon$ for tent map with bounded return time $T(x_n) = 1 + \varepsilon \sin 2\pi x_n$.

As discussed in the Introduction, this type of singularity of $T(x)$ occurs in continuous time systems when the orbit of a point $\overline{x}$ on a Poincaré surface of section P approaches a steady state x_* embedded in the attractor but located off P. The point $\overline{x}$ represents the intersection of the stable manifold of x_* with P; if the stable manifold is more than one dimensional, the intersection will be a curve or a higher-dimensional subsurface of P.

In order to determine the appropriate form of $T(x)$ as $x \to \overline{x}$, we consider in more detail the dynamics of such a continuous time system. Consider a trajectory $\tilde{x}(t)$ where $\tilde{x}(0) = x$ is a point on the Poincaré section P near $\overline{x}$. Fix a small neighborhood N of the steady state x_*. The amount of time taken by $\tilde{x}(t)$ to reach N is bounded as x approaches $\overline{x}$, as is the time taken to return from the boundary of N back to P. Thus the growth of $T(x)$ toward infinity as $x \to \overline{x}$ is due entirely to the amount of time spent by $\tilde{x}(t)$ in N.

Now since the steady state x_* is embedded in a chaotic attractor, it must be a saddle point, whose stable manifold S intersects P at $\overline{x}$ (and perhaps at some curve or higher-dimensional subsurface through $\overline{x}$). If $\tilde{x}(0) = x$ is close to $\overline{x}$, then it is close to S and the distance of $\tilde{x}(t)$ from S grows approximately exponentially (with growth rate independent of $|x - \overline{x}|$) as long as this distance remains small. In order for $\tilde{x}(t)$ to exit the neighborhood N of x_*, its distance from S must grow to be approximately the radius of N. Since at time 0 this distance is $|x - \overline{x}|$, the time at which $\tilde{x}(t)$ exits N is (to first order) proportional to $\ln(1/|x - \overline{x}|)$. Therefore, $T(x)$ grows as $C \ln(1/|x - \overline{x}|)$ as $x \to \overline{x}$.

Another complication introduced by the existence of the embedded steady state x_* is that the optimal performance average may occur at x_* rather than on a trajectory that returns to the Poincaré section P. Based on the discussion above of the dynamics near the stable manifold of x_*, notice that the fraction of the return time $T(x)$ that $\tilde{x}(t)$ spends in N approaches 1 as $x \to \overline{x}$. It follows that the average $\tilde{F}(x)$, defined by Eq. (2), of the performance function F over this time period converges to $F(x_*)$ as $x \to \overline{x}$. Thus we define $\tilde{F}(\overline{x}) = F(x_*)$, and, in computing the optimal average of $\tilde{F}$ with respect to the dynamics on P, we treat $\overline{x}$ as a special ''period 0'' orbit, corresponding to the steady state at x_*, to be compared with the orbits of period 1,2,3, . . . that return to P.

A. Doubling transformation

We consider again the doubling transformation (7) with the average given by Eq. (4) and Eq. (6), but with a new family of return time functions which we choose based on the discussion above:

$$T_\varepsilon(x) = 1 + \varepsilon \ln \frac{1}{|\sin \pi(x - 1/2)|}. \tag{9}$$

Here we imagine $\overline{x} = 1/2$, the point of discontinuity for Eq. (7), to represent a point on a Poincaré surface of section whose trajectory approaches an unstable fixed point x_* off the surface of section. Larger values of ε correspond to larger amounts of time spent near x_*, i.e., smaller values of the unstable eigenvalue(s) for x_*.

For a given value of ε, our numerical experiment is the same as in the previous section; for each of 10^5 evenly spaced values of γ, we find the maximum of $\langle F_\gamma \rangle_\varepsilon$ defined by Eq. (6) over all periodic orbits of Eq. (7) with period at most 24, including now the period 0 point $\overline{x}$. The optimal period as a function of γ is shown for $\varepsilon = 0.1$, $\varepsilon = 0.5$, and $\varepsilon = 10$ in Fig. 5. The solid line represents the optimal period excluding period 0, and the dotted line includes period 0. Notice that when the values of ε are large, for a substantial set of γ values near 0.5, the optimal period excluding 0 is 24. However, when we include the period 0 point, we see that the optimum is as before achieved at low period for most values of γ. We observe a similar effect in the next section for the Lorenz system.

Furthermore, we find (as in the case of bounded return time) that, regardless of the value of ε, the fraction $r(p)$ of γ values with optimal period at least p decreases as $p^2 2^{-p}$ as p increases. The graph of $r(p)/p^2$ versus p for various ε is shown in Fig. 6.

B. Tent Map

Next we show the analogous results for the tent map (8), again with the family of performance functions F_γ given by Eq. (4), but with a slightly different family of return time functions,

$$T_\varepsilon(x) = 1 + \varepsilon \ln \frac{1}{2|x - 1/2|}. \tag{10}$$

In Fig. 7 we show the periods of the orbits that maximize $\langle F_\gamma \rangle_\varepsilon$, as defined in Eq. (6), as a function of γ for $\varepsilon = 0.1$, $\varepsilon = 0.5$, and $\varepsilon = 10$. As for the doubling transformation, the period 0 point is optimal for an interval of γ values that does not change dramatically for differing values of ε. And for larger values of ε we see again that for many of these γ values the optimum among the positive values of the period p is the largest period 24, representing an orbit that spends as much time as possible near the critical point $\overline{x} = 1/2$.

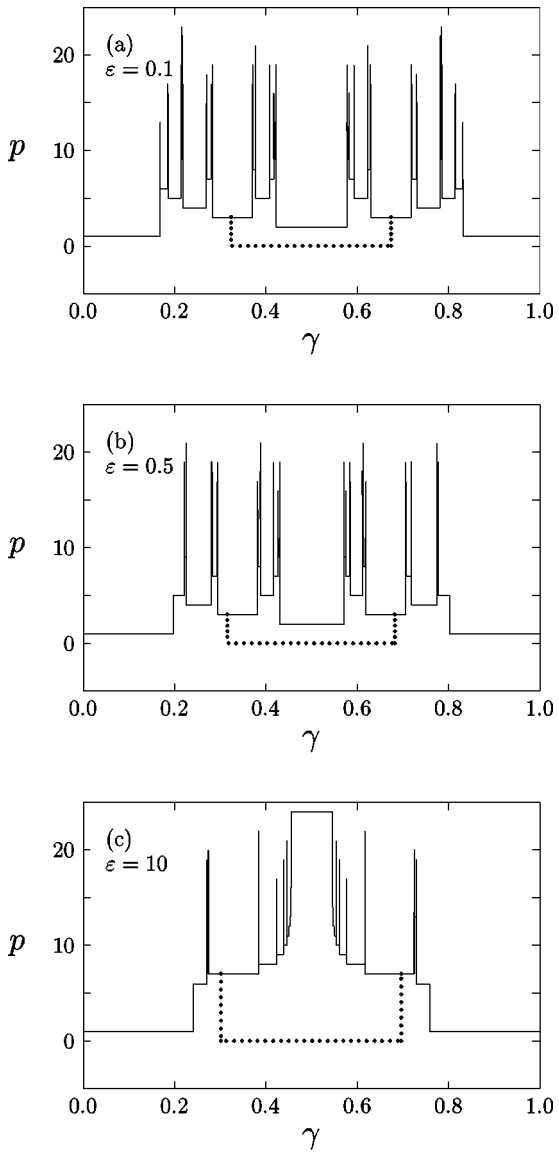

FIG. 5. Periods that optimize $\langle F_\gamma \rangle_\varepsilon$ for the doubling transformation with unbounded return time $T(x_n) = 1 + \varepsilon \ln|\sin \pi(x_n - \overline{x})|^{-1}$ for (a) $\varepsilon = 0.1$, (b) $\varepsilon = 0.5$, and (c) $\varepsilon = 10$. The graph is based on computations using 10^5 evenly spaced values of γ and orbits of periods from 0 to 24 (dotted line) or from 1 to 24 (solid line). For most of the values of γ, the solid line and the dotted line coincide.

IV. CONTINUOUS TIME SYSTEM: LORENZ EQUATIONS

Finally, we consider the Lorenz equations [13,14],

$$\frac{dx}{dt} = -\sigma x + \sigma y,$$

$$\frac{dy}{dt} = -xz + Rx - y, \tag{11}$$

$$\frac{dz}{dt} = xy - \beta z,$$

where σ, R, and β are dimensionless parameters, which we set to the original values used by Lorenz, $\sigma = 10$, $R = 28$, and $\beta = 8/3$.

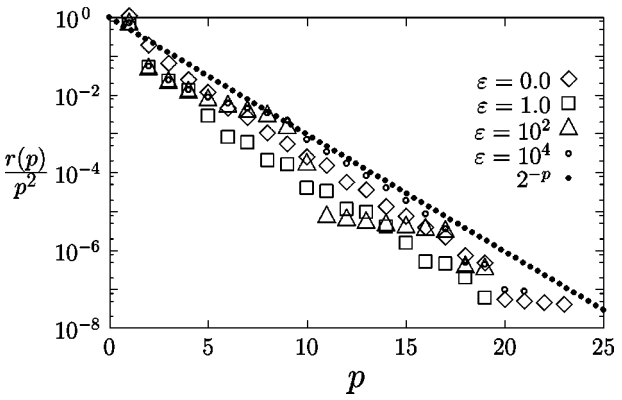

FIG. 6. Comparison of $r(p)/p^2$ with 2^{-p}, where $r(p)$ is the fraction of γ values for which period p or larger optimizes $\langle F_\gamma \rangle_\varepsilon$ for the doubling transformation with unbounded return time $T(x_n) = 1 + \varepsilon \ln|\sin \pi(x_n - \overline{x})|^{-1}$.

A. Finding periodic orbits by symbolic dynamics

To facilitate the determination of periodic orbits of Eq. (11) we utilize symbolic dynamics and a convenient choice of the surface of section. In particular, the surface of section is chosen as the strip

$$\{z = R - 1, \ -2\sqrt{\beta(R-1)} < x + y < 2\sqrt{\beta(R-1)}\}. \tag{12}$$

There are two unstable fixed points on the edges of this strip. One, C_1, is located at $(\sqrt{\beta(R-1)}, \ \sqrt{\beta(R-1)}, \ R-1)$ and the other, C_2, is located at $(-\sqrt{\beta(R-1)}, \ -\sqrt{\beta(R-1)}, \ R-1)$. All trajectories on the attractor pass through this strip going downward, $dz/dt < 0$. Figure 8 shows the attractor (dark solid lines) in the surface of section. The attractor in the surface of section appears to be approximately one dimensional (two arcs), and in what follows we make use of this approximate one-dimensionality. (Actually, of course, there is some small thickness to these arcs inside which fractal structure is present. We neglect this in what follows.)

There are two particular points (marked a and d in Fig. 8) on the attractor, such that the trajectories through them go to the other fixed point C_0 located at the origin $(0,0,0)$. We pick two directions, $\mathbf{e}_1$ at 45° to the x axis, and $\mathbf{e}_2$ along the line ad in Fig. 8. Transforming to a coordinate system where $\mathbf{e}_1$ and $\mathbf{e}_2$ are perpendicular, and defining the angle $2\pi\theta$ from $\mathbf{e}_1$ in that system, we arrive at a one-dimensional map, θ_{n+1} versus θ_n, by recording data from a long orbit on the attractor (see Fig. 9). This map takes the interval $(0,1)$ to itself, and this interval is conveniently divided into four parts $A = (0,1/4)$, $B = (1/4,1/2)$, $C = (1/2,3/4)$, $D = (3/4,1)$. The possible transitions of an orbit visiting these intervals are shown in Fig. 10.

We wish to find the periodic orbits of the one-dimensional map in Fig. 9. For this purpose we use cubic spline fits of the numerical data in Fig. 9. Because all the periodic points embedded in the Lorenz chaotic attractor are unstable, a convenient way of finding them is via backward iteration of the map. However, since the map is noninvertible, to iterate the map backward we need to choose, at each iteration, the branch of the inverse in an appropriate way. To do this, we use the symbolic dynamical rules shown in Fig. 10. Given a

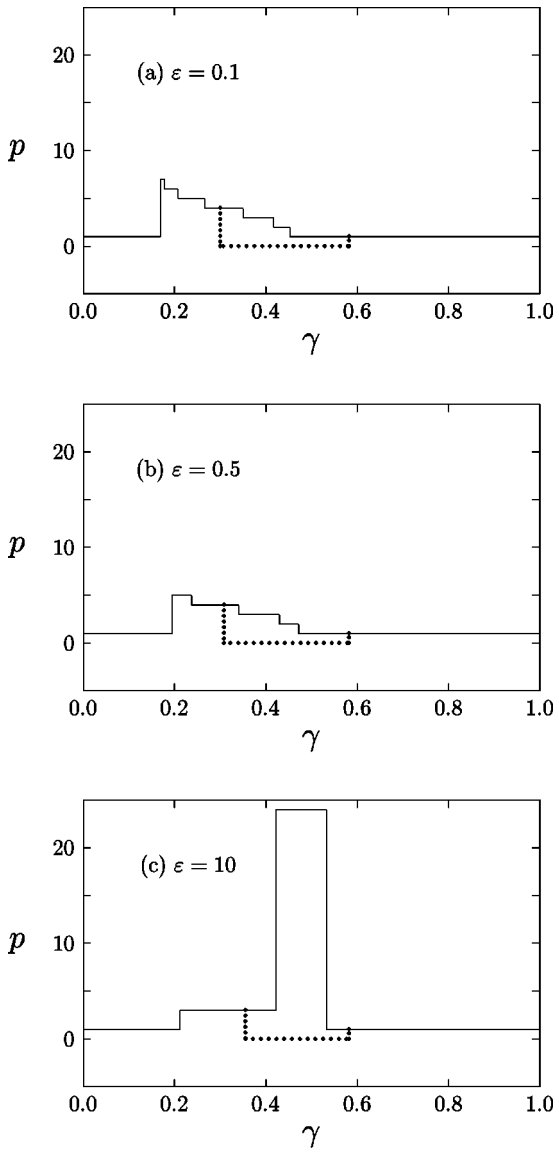

FIG. 7. Periods that optimize $\langle F_\gamma \rangle_\varepsilon$ for the tent map with unbounded return time for (a) $\varepsilon = 0.1$, (b) $\varepsilon = 0.5$, and (c) $\varepsilon = 10$. The dotted line represents the maximum from $p = 0$ to 24, and the solid line represents the maximum from $p = 1$ to 24.

periodic symbolic sequence of A's, B's, C's, and D's that is allowed by Fig. 10, we start with an arbitrary initial condition in one of the intervals and follow the symbolic sequence backward to choose successive branches of the inverse map. Because of the forward instability, this procedure converges to the unique periodic orbit with the given symbol sequence, if one exists. Thus we can efficiently locate all periodic orbits of the map with a given period by searching the possible symbol sequences with that period. (Not all symbol sequences allowed by the transition diagram Fig. 10 actually occur as orbits of the map Fig. 9. For example although it is hard to tell from Fig. 9, the return map does not quite touch the diagonal, and thus it has no fixed points corresponding to the symbol sequences $BBBB\ldots$ and $DDDD\ldots$, which are allowed by Fig. 10. Further, as we will show later, periodic orbits with a consecutive string of more than 25 B's or D's do not occur.)

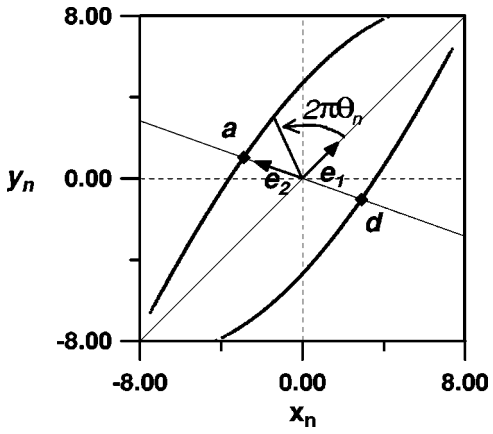

FIG. 8. The Poincaré section of the Lorenz attractor. Points a and d are two critical points on the section. Any trajectories going through points a or d will approach the fixed point at (0,0,0). We construct an approximate one-dimensional (1D) return map using the angular coordinate $2\pi\theta$. This angle is measured from the positive $\mathbf{e}_1$ direction after a change of variables that makes $\mathbf{e}_1$ and $\mathbf{e}_2$ perpendicular.

B. Optimal invariant sets

After detecting the locations of the periodic orbits embedded in the Lorenz attractor, the optimal average performance function is evaluated. Here, the definition of the average performance function is as given in Eqs. (2) and (3), which we rewrite below in slightly different notation [in Eqs. (2) and (3), x is a vector, while below x, y, and z are scalars, as in Eq. (11)].

$$\langle F_\gamma \rangle \equiv \lim_{N\to\infty} \frac{\sum_{n=1}^{N} T(x_n,y_n)\tilde{F}_\gamma(x_n,y_n)}{\sum_{n=1}^{N} T(x_n,y_n)}, \tag{13a}$$

$$\tilde{F}_\gamma(x_n,y_n) \equiv \frac{1}{T(x_n,y_n)} \int_0^{T(x_n,y_n)} F_\gamma(x(t),y(t),z(t))dt, \tag{13b}$$

where $x_n = x(0)$, $y_n = y(0)$, and $z_n = z(0)$ are, respectively, the x, y, and z coordinates of the points on the Poincaré section. The performance function is chosen to be

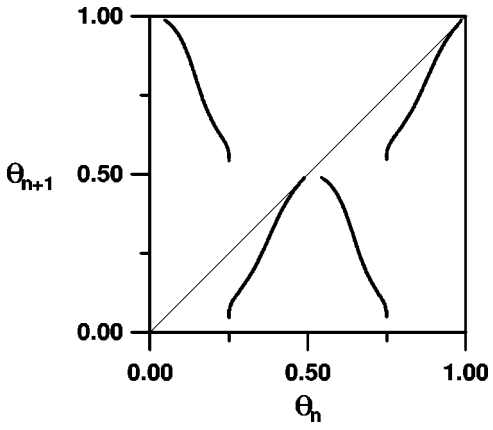

FIG. 9. The approximate 1D return map obtained from the Lorenz system.

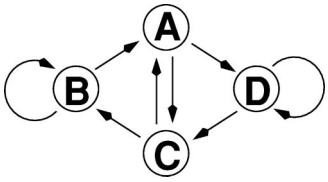

FIG. 10. Symbolic diagram for the 1D return map shown in Fig. 9.

$$F_\gamma(x(t),y(t),z(t))=(\cos 2\pi\gamma)z(t)+(\sin 2\pi\gamma)y(t), \tag{14}$$

where γ is a parameter in $[0,1]$. Figure 11 shows a plot of the optimal periods that maximize Eq. (13a) as a function of the parameter γ. The plot was obtained using 10^4 evenly spaced values of γ in $[0,1]$, and all the periodic orbits of the Lorenz equations (11) with return map periods from 1 to 16. In the range $0.44<\gamma<0.56$, a Farey tree structure similar to that found in the previous cases can be discerned. Outside this γ range, among the periods tested, the highest period ($p=16$) is optimal. Thus the optimal orbit has $p\geqslant 16$. A similar tendency toward high optimal period for the Lorenz equations has been found by Zoldi and Greenside [15] with a different performance function. [Note, however, that if the unstable fixed point at $(0,0,0)$ is considered, it dominates the Farey tree structure and is optimal for about $0.29<\gamma<0.71$ (dotted line in Fig.11).]

The fact that optimality occurs for the highest period tested ($p=16$) apparently brings our conjectures (i)–(iii) in Sec. I into question. We show below, however, that conjectures (i)–(iii) are still expected to apply. In particular, with regard to conjecture (i), optimality still occurs at finite period, namely, $p\cong 25$. We also show that the reason for this occurrence of a relatively large optimizing period is that, for the standard parameter choice $R=28$, the Lorenz system is near a crisis. Thus, with regard to conjecture (ii), we will show that for most values of R in the range for which the Lorenz system is chaotic, optimality is likely to occur at low period. Furthermore, we demonstrate below that as a system approaches a crisis, the optimal period approaches infinity in the following way: if Δ_p is the parameter range over which a period p orbit is optimal, then as p gets larger Δ_p becomes smaller exponentially fast, $\ln\Delta_p\simeq-(const)\,p$. Thus, enlarging the meaning of typicality in conjecture (ii) of Sec. I to include variation of a system parameter (R in this case) as well as variation of a performance function parameter (γ in this case), it is still the case that optimality typically occurs at low period (or on a steady state).

To see what the characteristics of the optimal orbits are, the period 2 and period 16 optimal orbits for Eq. (14) (for γ near 0.5 and γ near 0, respectively) are shown in Fig. 12. The period 16 orbit spends much of its time close to the fixed point C_2, which is near to but not on the attractor. (There is also a symmetric orbit that is concentrated near C_1.)

More generally, when the average performance is greater at C_1 or C_2 than for any orbit on the attractor, we can expect the optimal orbit to be the one that spends as large a proportion of time as possible near one of these fixed points. Thus we expect that at the usual Lorenz parameter values, there is a symmetric pair of relatively high-period orbits on the attractor that will be optimal for a large class of performance functions. To get an idea of the period of these orbits, and how their period depends on system parameters, we consider the symbolic dynamics of the Lorenz attractor as a function of the system parameter R.

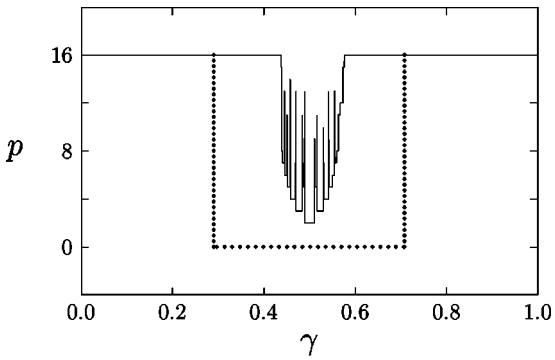

FIG. 11. The optimal periods for the Lorenz system that maximize the average performance function Eq. (14). The dotted line is the result when the period 0 fixed point (0,0,0) is included, while the solid line shows the result of not considering the fixed point.

To define the symbolic coding for a trajectory, consider the sign of x when z reaches a local maximum. If $x<0$, we record a 0, whereas if $x>0$, we record a 1. Because z has a local maximum exactly once between any two consecutive piercings of the Poincaré surface of section, we record one symbol for each iteration of the Poincaré return map. For example, the orbit in Figs. 12(a,b) has symbolic coding 01010101 . . . , whereas the coding for the orbit in Figs. 12(c,d) consist of a repeating string of 16 symbols: a 0 followed by 15 1's. See [14] for more about the symbolic dynamics of the Lorenz system and [9] for a discussion of the symbolic dynamics of optimal orbits.

In terms of this symbolic coding, we are interested in describing, as a function of R, the period of the orbit with the maximum proportion of 0's in its symbolic coding (the symmetric orbit will have the maximum proportion of 1's). Now, as R decreases through a critical value $R_c\approx 24.06$, the system undergoes a ''crisis'' at which the attractor collides with two unstable periodic orbits near the two fixed points C_1 and C_2, and the attractor is destroyed as almost all trajectories approach one of these fixed points [16]. In [17] it is shown for the standard tent map that, near a crisis, for most parameter values the symbolic coding of the orbit that has the greatest proportion of 0's consists of $\ell=p-1$ consecutive 0's followed by a 1, where p is the period of the orbit, and p grows to infinity as the crisis parameter value is approached. Likewise, we expect the same symbolic dynamics for the orbit with the greatest proportion of 0's in the Lorenz attractor, for most values of R.

In order to understand this behavior it is useful (as in Lorenz's paper) to consider the essentially one-dimensional map z_{n+1} versus z_n, where z_n denotes the nth maximum of $z(t)$; see the schematic illustration in Fig. 13. In this map both of the unstable periodic orbits encircling C_1 and C_2 are represented by the same fixed point, $z=z_\alpha$. Also, a periodic orbit that circles C_1 (or C_2) $p-1$ times and then circles C_2 (or C_1) one time corresponds to an orbit of this map that spends $p-1$ iterates with $z<z_*$ and one iterate with $z>z_*$. From Fig. 13 we see that the chaotic attractor for the

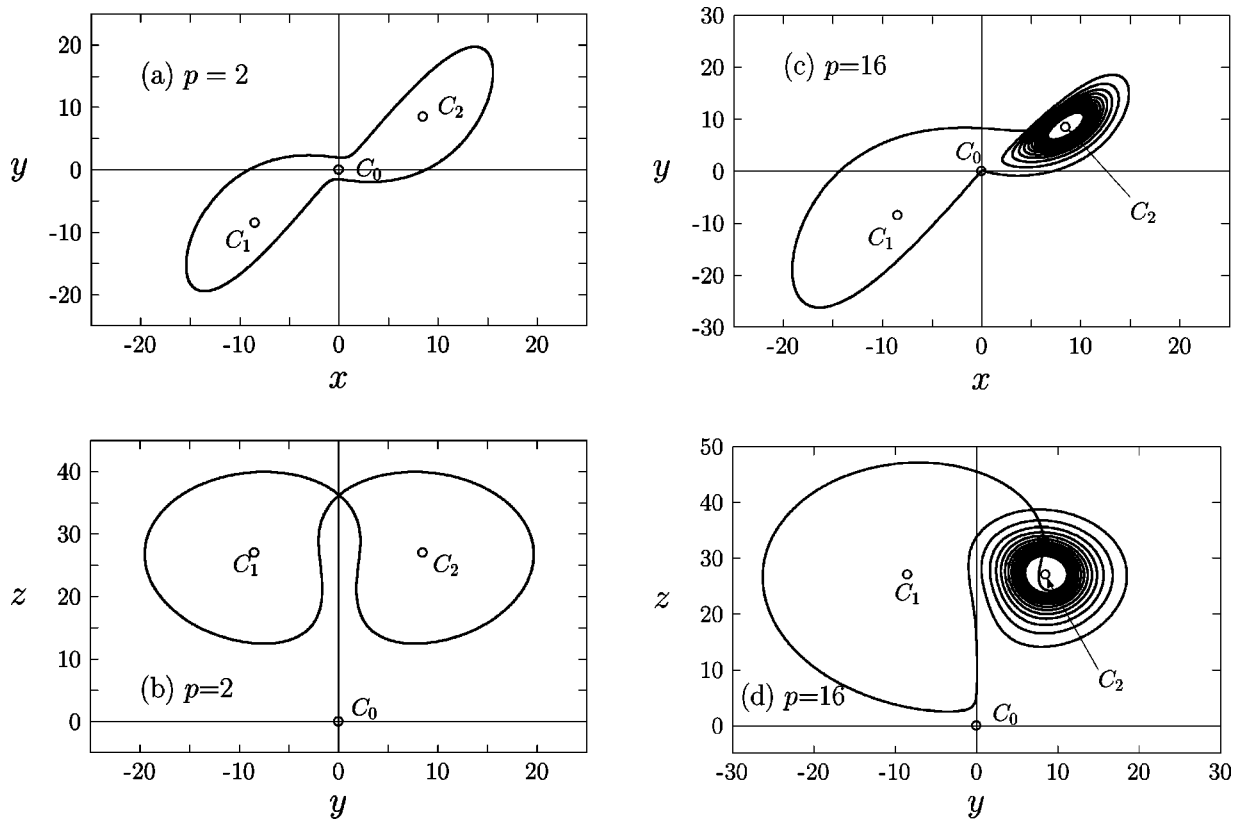

FIG. 12. The trajectories of the optimal periods that maximize the average performance function Eq. (14): (a) period 2, projected on the X-Y plane, (b) period 2, projected on the Y-Z plane, (c) period 16, projected on the X-Y plane, and (d) period 16, projected on the Y-Z plane.

map is confined to the region $z_\gamma \geqslant z \geqslant z_\beta > z_\alpha$. Hence p is at most 1 greater than the number ℓ of iterates starting from $z_1 = z_\beta$ that the map orbit spends in $z < z_*$. As the crisis is approached ($R \to R_c$), z_γ increases and $z_\beta \to z_\alpha$ (i.e., the attractor collides with the unstable period 1 orbit). At $R = R_c$, $z_\beta = z_\alpha$, and $\ell = \infty$, because z_β is an unstable fixed point of the map.

Thus we consider, as a function of R, the maximum number ℓ of consecutive 0's (or 1's) that the symbolic dynamics of a trajectory on the Lorenz attractor generate. This corresponds to the maximum number of consecutive loops a trajectory on the attractor can make around the same fixed point, C_1 or C_2, before looping closer to the other fixed point. Figure 14 shows our numerical results. Indeed, for the smaller values of R near the crisis parameter value, ℓ can be fairly large, indicating that orbits with period $p = \ell + 1$ are likely to be optimal for many performance functions. (For the value $R = 28$ used by Lorenz, our results yield $\ell + 1 = 26$.) As was found in [17] for the tent map, we observe that, for large p, the length of the parameter interval corresponding to p decays exponentially as p increases to infinity. Thus, as previously discussed, optimality occurs for low period in the sense that the Lebesgue measure of the set of parameter values for which the optimal period is p decays exponentially with increasing p.

As R increases, the attractor pulls away from the fixed points C_1 and C_2, and for most values of R, shown in Fig. 14, the maximum number ℓ of consecutive loops around one of these fixed points is less than 10, indicating that high-period orbits are unlikely to be optimal for typical performance functions.

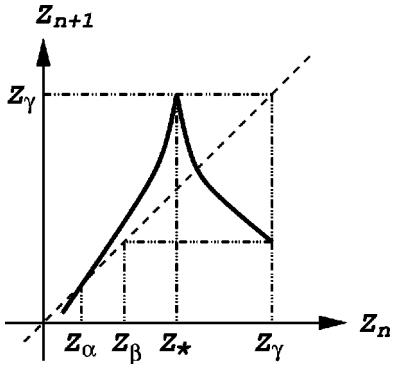

FIG. 13. Schematic one-dimensional map z_{n+1} versus z_n, where z_n denotes the nth maximum of $z(t)$ in Eq. (11).

C. Near crisis

We now vary the parameter in the standard tent map [Eq. (15)] in order to illustrate the effect that near a crisis the system parameter measure for which high-period orbits are optimal decreases exponentially as the crisis is approached. Consider the tent map

$$x_{n+1} = \begin{cases} \gamma x_n, & 0 \leqslant x_n \leqslant 1/2 \\ \gamma(1 - x_n), & 1/2 \leqslant x_n \leqslant 1, \end{cases} \tag{15}$$

where $\gamma \leqslant 2$ is a real parameter. The attractor for this map is the interval

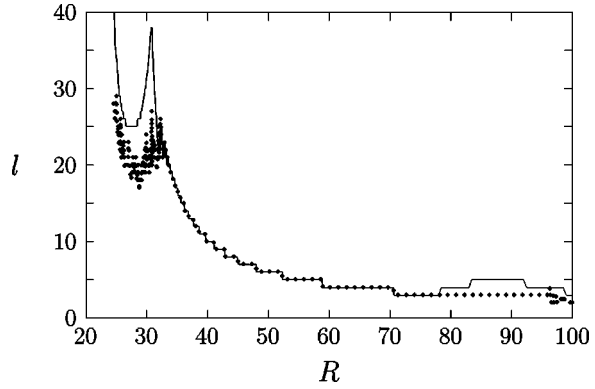

FIG. 14. The greatest number of consecutive z maxima of the Lorenz system for which the sign of x remains the same, as a function of the system parameter R. The solid line is the result of starting the trajectory very close to (0,0,0) and recording the z maxima immediately, without dropping any transient part of the trajectory. This line is likely to be most valid for smaller values of R, when the fixed point (0,0,0) belongs to the attractor. (Since this fixed point is at the edge of the attractor, its unstable manifold passes along the outside of one lobe of the attractor and then to the inside of the other lobe, so that it will remain in this lobe at least as long as any other trajectory on the attractor.) The dotted line is the result of starting from a random chosen initial point and letting the trajectory stabilize on the chaotic attractor before recording the z maxima. This line is likely to be most valid for larger values of R, when the whole attractor can be explored in a reasonable amount of time. In both cases, for each value of R from 24.5 to 100 in increments of 0.1, we recorded 5×10^4 z maxima.

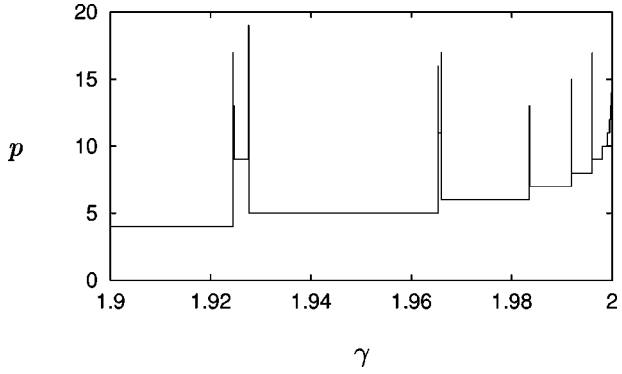

FIG. 15. Optimal period p for $\langle 1-x\rangle$ as a function of the tent map parameter γ.

$$\gamma(1-\gamma/2)\leqslant x\leqslant \gamma/2, \tag{16}$$

and it undergoes a crisis as $\gamma\to2$, colliding with the fixed point $x=0$. The maximum number n of iterations for which an orbit within the attractor can stay between 0 and 1/2 is given by

$$\gamma^n(1-\gamma/2)\leqslant 1/2<\gamma^{n+1}(1-\gamma/2). \tag{17}$$

Thus n increases as γ approaches the crisis value 2, and the Lebesgue measure of parameter values γ corresponding to a given n decreases exponentially as 2^{-n}. Likewise we expect that for a performance function that is largest at $x=0$ (much as $\langle N\rangle$ in the Lorenz case is largest at a fixed point outside the attractor [15]), the Lebesgue measure of parameters for which the optimal periodic orbit *within the attractor* has period greater than p decreases exponentially as p increases. Figure 15 shows the period that maximizes $\langle 1-x\rangle$, among all orbits with period at most 24, for 10^4 evenly spaced values of the parameter γ between 1.9 and 2. For most of these parameter values, the optimal periodic orbit is indeed found to be the orbit of period $n+1$ that spends n iterations between 0 and 1/2 followed by one iteration between 1/2 and 1, where n is given by the formula in Eq. (17).

V. CONCLUSION

In this paper we have considered optimal periodic orbits on chaotic attractors of continuous time systems. Our main result is that optimality is typically achieved either on a periodic orbit or on a steady state. We also find that, in some circumstances, the optimal period becomes larger and larger as a crisis is approached.

ACKNOWLEDGMENTS

T.-H. Y. gratefully acknowledges support from the Ministry of Education, Taiwan, during his stay at the University of Maryland, and the National Science Councils, Taiwan, under Contract No. NSC87-2112-M-009-017. This work was also supported by the Office of Naval Research (Physics Division), the U.S. Department of Energy (Mathematical, Information, and Computational Sciences Division, High Performance Computing and Communications Program), and the National Science Foundation (Divisions of Mathematical Sciences and Physics).

[1] E. Ott, C. Grebogi, and James A. Yorke, Phys. Rev. Lett. **64**, 1196 (1990).
[2] U. Dressler and G. Nitsche, Phys. Rev. Lett. **68**, 1 (1992).
[3] W.L. Ditto, S.N. Rauseo, and M.L. Spano, Phys. Rev. Lett. **65**, 3211 (1990).
[4] J. Singer, Y.-Z. Wang, and H.H. Bau, Phys. Rev. Lett. **66**, 1123 (1991).
[5] E.R. Hunt, Phys. Rev. Lett. **67**, 1953 (1991).
[6] V. Petrov, V. Gáspár, J. Masere, and K. Showalter, Nature (London) **361**, 240 (1993).
[7] In other scenarios, optimality may correspond to minimizing the time average of some function F. Since this is equivalent to maximizing the time average of $-F$, without loss of generality we consider in this paper only the case of maximizing a time average.
[8] B.R. Hunt and E. Ott, Phys. Rev. Lett. **76**, 2254 (1996).
[9] B.R. Hunt and E. Ott, Phys. Rev. E **54**, 328 (1996).
[10] T. Sauer, J.A. Yorke, and M. Casdagli, J. Stat. Phys. **65**, 579 (1991).
[11] B.R. Hunt, Nonlinearity **9**, 845 (1996).

[12] P. Ashwin, J. Buescu, and I. Stewart, Phys. Lett. A **193**, 126 (1994); S.C. Venkataramani, B.R. Hunt, and E. Ott, Phys. Rev. E **54**, 1346 (1996); S.C. Venkataramani, B.R. Hunt, E. Ott, D.J. Gauthier, and J.C. Bienfang, Phys. Rev. Lett. **77**, 5361 (1996).
[13] E.N. Lorenz, J. Atmos. Sci. **20**, 130 (1963).
[14] C. Sparrow, *The Lorenz Equations: Bifurcations, Chaos, and Strange Attractors* (Springer-Verlag, New York, 1982).
[15] S.M. Zoldi and H.S. Greenside, Phys. Rev. Lett. **80**, 1790 (1998).
[16] J. A. Yorke and E. D. Yorke, J. Stat. Phys. **21**, 263 (1979); C. Grebogi, E. Ott, and J. A. Yorke, Physica D **7**, 181 (1983).
[17] B.R. Hunt and E. Ott, Phys. Rev. Lett. **80**, 1791 (1998).